EUROPHYSICS LETTERS 15 August 2003

Europhys. Lett., **63** (4), pp. 569–575 (2003)

Spin and charge dynamics of stripes in doped Mott insulators

F. F. Assaad[1,2], V. Rousseau[3], F. Hebert[4], M. Feldbacher[1] and G. G. Batrouni[3]

[1] *Institut für Theoretische Physik III, Universität Stuttgart Pfaffenwaldring 58, D-70550 Stuttgart, Germany*
[2] *Max Planck Institute for Solid State Research Heisenbergstr. 1, D-70569 Stuttgart, Germany*
[3] *Institut Non-Linéaire de Nice, Université de Nice-Sophia Antipolis 1361 route des Lucioles, 06560 Valbonne, France*
[4] *Theoretische Physik, Universität des Saarlandes - 66041 Saarbrücken, Germany*

(received 25 November 2002; accepted in final form 10 June 2003)

PACS. 71.27.+a – Strongly correlated electron systems; heavy fermions.
PACS. 71.10.Fd – Lattice fermion models (Hubbard model, etc.).

Abstract. – We study spin and charge dynamics of stripes in doped Mott insulators by considering a two-dimensional Hubbard model with N fermion flavors. For $N = 2$ we recover the normal one-band model while for $N \to \infty$ a spin density wave mean-field solution. For all band fillings, lattice topologies and $N = 4n$, the model may be solved by means of quantum Monte Carlo methods without encountering the sign problem. At $N = 4$ and in the vicinity of the Mott insulator we find a stripe phase. This phase has a quasiparticle gap but conducts due to long-wavelength low-lying collective charge modes.

The understanding of the interplay between spin and charge degrees of freedom in doped two-dimensional Mott insulators remains a challenging issue. On the analytical front, it is straightforward to apply the Hartree-Fock (HF) approximation, but the difficulty lies in taking quantum fluctuations into account. On the other hand, numerical methods take into account fluctuations but are limited to small clusters due to the size of the Hilbert space, for exact diagonalization, or due to the minus-sign problem inherent to quantum Monte Carlo (QMC) methods. In this letter, we introduce a QMC method which lies between HF and full quantum fluctuations and apply it to the doped two-dimensional Hubbard model. Since the N-flavor model we consider breaks $SU(N)$ spin symmetry, it favors spin states. In particular, in the vicinity of the Mott insulator (MI) we find a stripe phase experimentally observed in cuprates and nickelates [1, 2]. Our simulations reveal the dynamics of this phase.

Our starting point is the Hamiltonian

$$H = -t \sum_{(\vec{i},\vec{j})} \boldsymbol{c}^{\dagger}_{\vec{i}} \boldsymbol{c}_{\vec{j}} - \frac{U}{N} \sum_{\vec{i}} \left(\boldsymbol{c}^{\dagger}_{\vec{i}} \boldsymbol{\lambda} \boldsymbol{c}_{\vec{i}} \right)^2, \tag{1}$$

where $\vec{i}$ labels the sites of a square lattice and the first sum runs over nearest neighbors. The spinors $\boldsymbol{c}^\dagger_{\vec{i}} = (c^\dagger_{\vec{i},1} \cdots c^\dagger_{\vec{i},N})$ correspond to fermions with N flavors. For even values of N, $\lambda_{\alpha,\gamma} = \delta_{\alpha,\gamma} f(\alpha)$ with $f(\alpha) = 1$ for $\alpha \leq N/2$ and -1 otherwise. At $N = 2$, the model reduces to the standard $SU(2)$-spin-invariant Hubbard model since the interaction is the square of the magnetization. Away from $N = 2$, the model has an $SU(N/2) \otimes SU(N/2)$ symmetry which becomes clear when writing the Hamiltonian in terms of the spinors: $(c^\dagger_{\vec{i},1} \cdots c^\dagger_{\vec{i},N/2})$ and $(c^\dagger_{\vec{i},N/2+1} \cdots c^\dagger_{\vec{i},N})$. For $N \to \infty$, we will show below that the exact solution of the model is a spin-density wave mean-field approximation of the $N = 2$ model based on the ansatz $\langle n_{\vec{i},1} - n_{\vec{i},2} \rangle = m_i$.

The central observation is that at $N = 4n$ the minus-sign problem in the QMC approach is never present, regardless of the lattice topology and band filling. To illustrate this and to keep the notation simple, we consider the finite-temperature auxiliary field QMC approach. After the usual decoupling of the interaction term with a Hubbard-Stratonovich transformation, the partition function becomes $Z = \int \mathcal{D}\boldsymbol{\phi} e^{-NS(\boldsymbol{\phi})}$, where

$$\begin{aligned} S(\boldsymbol{\phi}) &= U \frac{\sum_{\vec{i}} \int_0^\beta \mathrm{d}\tau \phi^2_{\vec{i}}(\tau)}{4} - \frac{1}{2} \ln \mathrm{Tr} \left[T e^{-\int_0^\beta \mathrm{d}\tau H(\tau)} \right], \\ H(\tau) &= -t \sum_{(\vec{i},\vec{j}),\sigma=\pm} c^\dagger_{\vec{i},\sigma} c_{\vec{j},\sigma} - U \sum_i \phi_{\vec{i}}(\tau) \Big(n_{\vec{i},+} - n_{\vec{i},-} \Big). \end{aligned} \tag{2}$$

Here T corresponds to time ordering and in terms of our original fermions we can identify $c_{\vec{i},+} = c_{\vec{i},1}$ and $c_{\vec{i},-} = c_{\vec{i},N/2+1}$ and $n_{\vec{i},+} = c^\dagger_{\vec{i},+} c_{\vec{i},+}$, $n_{\vec{i},-} = c^\dagger_{\vec{i},+} c_{\vec{i},-}$. As $N \to \infty$, the integral over the fields ϕ is dominated by the saddle point configuration, $\phi^\star$, satisfying $\partial S(\phi)/\partial\phi|_{\phi=\phi^\star} = 0$. A time-independent solution is $\phi^\star_i = \langle n_{\vec{i},+} - n_{\vec{i},-} \rangle$, where the expectation value is taken with respect to the Hamiltonian in eq. (2). This is precisely the set of self-consistent equations obtained from the mean-field decoupling: $n_{i,+} - n_{i,-} = \phi^\star_i + [(n_{i,+} - n_{i,-}) - \phi^\star_i]$ for the Hamiltonian of eq. (1) at $N = 2$.

Since $H(\tau)$ in eq. (2) is quadratic in the fermion variables we can carry out the trace analytically to obtain

$$e^{-NS(\phi)} = e^{-NU \frac{\sum_{\vec{i}} \int_0^\beta \mathrm{d}\tau \phi^2_{\vec{i}}(\tau)}{4}} \big[\det M^+(\phi) \big]^{N/2} \big[\det M^-(\phi) \big]^{N/2}. \tag{3}$$

For even values of $N/2$ ($N = 4n$) the Boltzmann weight, $e^{-NS(\phi)}$, is positive and the sign problem never occurs regardless of doping and lattice topology. Here, we study the ground-state properties of the Hamiltonian (1) with the related projector auxiliary field QMC algorithm. The detail of how to apply this algorithm to our Hamiltonian may be found in ref. [3], where the authors consider a very similar model —at least from the technical point of view. Dynamical information is obtained by using the Maximum Entropy method [4].

To test and interpret our approach, we show in fig. 1 the static spin and charge structure factors,

$$S^{\mathrm{c}}_{\mathrm{s}}(q) = \sum_{\vec{r}} e^{i\vec{r}\vec{q}} \big\langle \big(n_{0,+} \pm n_{0,-} \big) \big(n_{r,+} \pm n_{r,-} \big) \big\rangle, \tag{4}$$

as well as the ground-state energy as a function of $1/N$ on a 4×4 lattice, $U/t = 4$ and two holes doped away from half-filling. The electron density is defined as $\langle n \rangle = \frac{1}{V} \sum_{\vec{i}} \langle n_{\vec{i},+} + n_{\vec{i},-} \rangle$, where V is the number unit cells $\vec{i}$. In spite of sign problems for $N \neq 4n$, the QMC data interpolate between the mean-field solution at $N = \infty$ and the exact diagonalization results

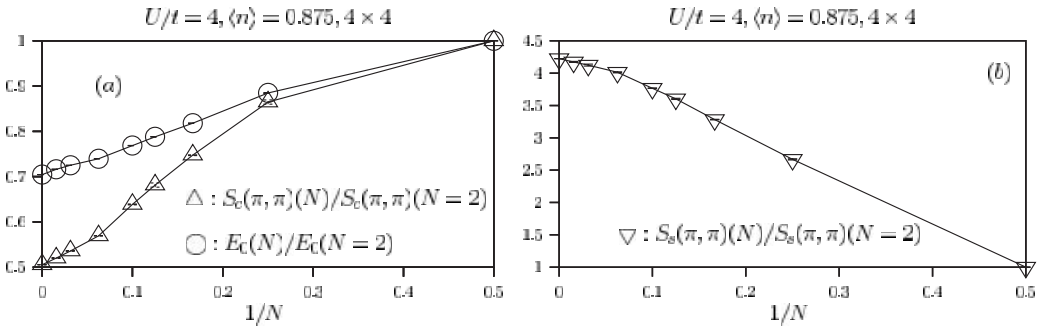

Fig. 1 – Ground-state energy as well as spin and charge structure factors at $\vec{q} = (\pi, \pi)$ as a function of $1/N$. The data points at $N = 2$ stem from exact diagonalization studies [5].

at $N = 2$. It is interesting to note that the sign problem becomes rapidly less and less severe for growing values of $N = 4n + 2$. In the context of the large-N approach [6], Gaussian fluctuations around the mean-field saddle point (*i.e.* the random phase approximation (RPA)) correspond to $1/N$ corrections. Figure 1 shows that for $N \geq 16$ we can understand our results in the framework of this approximation. The model at $N = 4$ may be seen as a model in its own right or in the framework of an approximation to the $N = 2$ Hubbard model which goes beyond the RPA approximation.

We use the method to investigate the metallic phase in the vicinity of the Mott insulator. To maximize quantum fluctuations, we concentrate on the $N = 4$ case. In the vicinity of the Mott insulating state, the relevant length scale is set by the inverse doping $1/\delta$. To achieve this length scale at least along one lattice direction, we will consider rectangular topologies of width ranging up to 10 lattice constants. We adopt periodic boundary conditions in both lattice directions.

We start with single-particle excitations. The density of states $N(\omega)$ as a function of doping is plotted in fig. 2 for various fillings. At $U/t = 3$, $N = 4$ and half-filling, we see a Mott gap of approximately $2t$ (fig. 2(a)). Upon doping, the chemical potential shifts into the lower Hubbard band and spectral weight is transferred from the upper Hubbard band to generate a low-energy feature [7]. In particular, at $\delta = 1/14$ remnants of the upper Hubbard band ($\approx 2t$ away from μ) are seen and a low-energy feature is detectable. The data of fig. 2 also show the presence of a small quasiparticle gap at finite dopings. This is confirmed by the single-particle occupation number $n(\vec{k})$ which shows a smooth behavior up to $\delta = 1/5$.

The origin of the quasiparticle gap lies in magnetic fluctuations which remain substantial away from half-filling. Figure 3 shows the spin and charge structure factors for several dopings δ on rectangles of width $L_y = 8$. For those topologies, the dominant features are along the $(1, 0)$ direction. In particular, we see a peak in the spin structure factor at $\vec{Q}_s = (\pi - \epsilon_x, \pi)$ accompanied by one in the charge structure factor at $\vec{Q}_c = (2\epsilon_x, 0)$ with $\epsilon_x = \pi\delta$. Transforming the data in real space yields the stripe caricature: rivers of holes along the y-direction separated by $1/\delta$ lattice constants in the x-direction. Across each river of holes, there is a π-phase shift in the spin structure with respect to the antiferromagnetic ordering. Similar features are seen in one dimension (1D), where our simulations at $N = 4$ show dominant cusps in the charge (spin) structure factors at $4k_f \equiv 2\pi\delta$ ($2k_f \equiv \pi - \pi\delta$) [8]. For $N = 4$, we verified that in 1D the $2k_f$ spin and $4k_f$ charge correlation functions both have power law decays. On fixed-width topologies one would equally expect power law decay of the correlation functions. We were however unable to confirm this numerically due to limitations on lattice sizes.

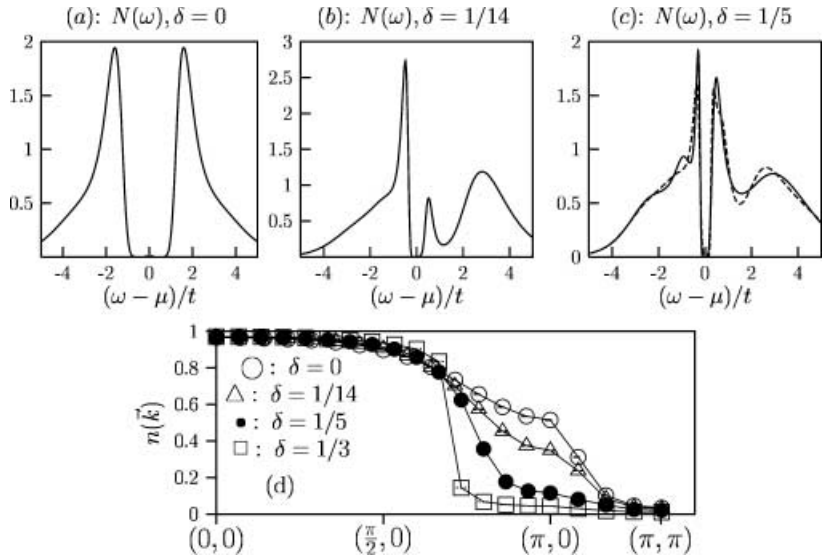

Fig. 2 – Density of states as a function of doping. The lattice sizes are: (a)-(b) 28×8, (c) 30×8 (solid line), 30×10 (dashed line). (d) Single-particle occupation number. We have set $U/t = 3$, $N = 4$ and $T = 0$.

To study the dynamical properties of the striped phase, we compute the imaginary-time displaced spin and charge correlation functions: $S_{\mathrm{c/s}}(\vec{q}, \tau)$. By fitting the tail $S_{\mathrm{c/s}}(\vec{q}, \tau)$ to a single exponential, we obtain the leading edge of the charge and spin excitation spectra: $\omega_{\mathrm{c/s}}(\vec{q})$. Irrespective of lattice width, the overall features of the QMC data of fig. 4 suggest gapless spin (charge) excitations with linear dispersions around $\vec{Q}_{\mathrm{s}}$ ($\vec{Q}_{\mathrm{c}}$ and $(0,0)$). The data equally show other features. i) At $L_y = 8, 10$, the spin and charge excitations lie below the particle-hole continuum which from the single-particle density of states (see fig. 2(c)) lies at a threshold energy $2\Delta_{qp} \approx 0.5t$. ii) The continuity equation, $\frac{\mathrm{d}}{\mathrm{d}t} n(\vec{x}, t) + \vec{\nabla} \cdot \vec{J}(\vec{x}, t) = 0$, yields an identity between the dynamical charge structure factor and the real part of the optical conductivity $\sigma'(\vec{q}, \omega)$: $\omega S_{\mathrm{c}}(\vec{q}, \omega)/q_x^2 \equiv \sigma'_{x,x}(\vec{q}, \omega)$. Assuming, and as suggested by our data, that for small values of q_x, $S_{\mathrm{c}}((q_x, 0), \omega) \propto q_x \delta(v_{\mathrm{c}} q_x - \omega)$ long-wavelength charge modes carry current so that we have a metallic state. This is confirmed by the optical conductivity QMC data of fig. 4(c). We have computed this quantity without including vertex corrections (solid line) to show that independent single-particle excitations are not responsible for the low-lying feature in $\sigma'_{x,x}$. Below we will consider the issue of the pinning of the charge density wave to the lattice.

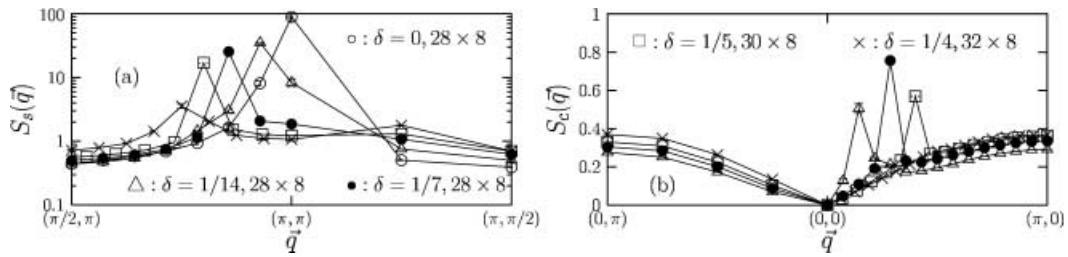

Fig. 3 – Spin (a) and charge (b) structure factors as a function of doping at $U/t = 3$.

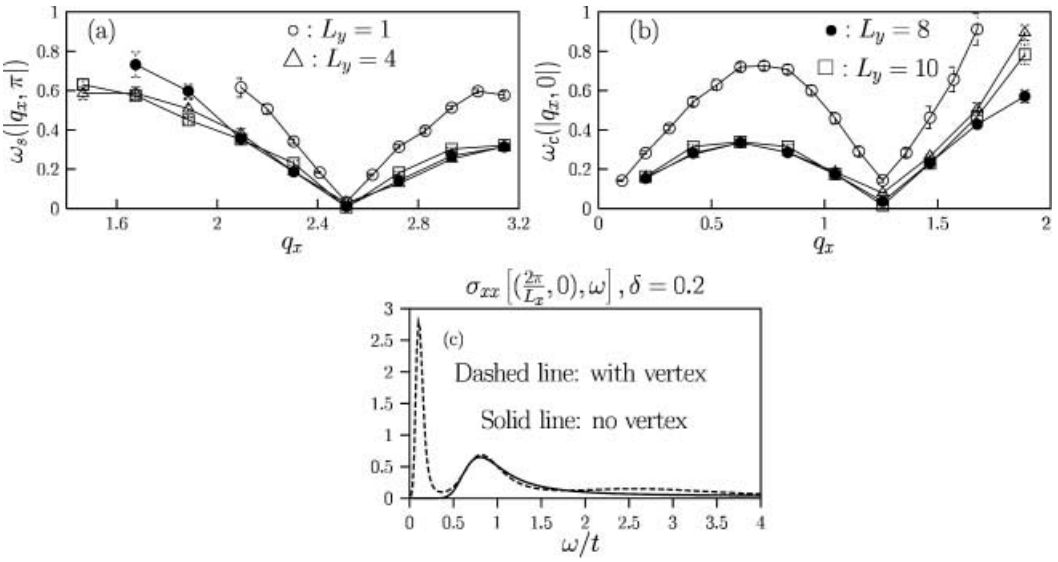

Fig. 4 – Leading edge of the spin (a) and charge (b) dynamical structure factor as a function of width L_y at $U/t = 3$, $\delta = 0.2$, $T = 0$ and $N = 4$. We consider $L_x = 60$ for $L_y = 1$ and $L_x = 30$ otherwise. Note that at $L_y = 1$, the second component of the wave vector has no meaning. (c) Optical conductivity with and without vertex contribution for the $L_y = 8$ lattice and at the largest wavelength in the x-direction.

We now consider possible interpretations of the data in terms of Goldstone modes. i) As mentioned previously, the model at $N = 4$ has an $SU(2) \otimes SU(2)$ symmetry and one may try to interpret the low-lying spin and charge features in terms of Goldstone modes associated with the breaking of this continuous symmetry. Since this symmetry leaves the Hamiltonian invariant under independent $SU(2)$ rotations of the spinors $(c^\dagger_{\vec{i},1}, c^\dagger_{\vec{i},2})$ and $(c^\dagger_{\vec{i},3}, c^\dagger_{\vec{i},4})$, we consider the pseudo-spin $\vec{T}_{\vec{i}} = \frac{1}{2}(c^\dagger_{\vec{i},1}, c^\dagger_{\vec{i},2})\vec{\sigma}(c_{\vec{i},1}, c_{\vec{i},2})^T$ as well as an equivalent pseudo-spin for the $(c^\dagger_{\vec{i},3}, c^\dagger_{\vec{i},4})$ spinor. Here $\vec{\sigma}$ denotes the Pauli spin matrices. Our calculations show that the correlation functions $\langle \vec{T}_{\vec{i}} \vec{T}_{\vec{j}} \rangle$ decay exponentially with distance $|\vec{i} - \vec{j}|$. Hence, the $SU(2) \otimes SU(2)$ symmetry is not broken and we can exclude this line of reasoning for the interpretation of the data. ii) Another possibility is to interpret our results in terms of phasons. We will assume long-range spin and charge density waves: $\langle n_{\vec{r},+} - n_{\vec{r},-} \rangle = \Delta_{\rm s} \cos(\vec{Q}_{\rm s}\vec{r} + \Phi_{\rm s})$ and $\langle n_{\vec{r},+} + n_{\vec{r},-} \rangle = \Delta_{\rm c} \cos(\vec{Q}_{\rm c}\vec{r} + \Phi_{\rm c})$ with $2\vec{Q}_{\rm c} = \vec{Q}_{\rm s}$. If the energy is invariant under translations of the spin and charge density waves: $\Phi_{\rm s} \to \Phi_{\rm s} + \Delta\Phi_{\rm s}$ and $\Phi_{\rm c} \to \Phi_{\rm c} + \Delta\Phi_{\rm c}$, then phasons may be seen as the Goldstone mode associated to this translation symmetry breaking [9, 10]. There are, however, two sources of pinning of the phase: impurities —not present in our numerical calculations— and commensuration with the lattice. For example, at half-band filling $\vec{Q}_{\rm s} = (\pi, \pi)$ and there is no charge density wave. In this case, the SDW order parameter $\langle \rho_{\rm s}(\vec{q}) \rangle \equiv (1/\sqrt{V}) \sum_{\vec{r}} e^{i\vec{q}\vec{r}} \langle n_{\vec{r},+} - n_{\vec{r},-} \rangle = \sqrt{V} \delta_{\vec{q},\vec{Q}_{\rm s}} \Delta_{\rm s} e^{i\Phi_{\rm s}}$. In this commensurate case, $\vec{Q}_{\rm s} = -\vec{Q}_{\rm s} + \vec{G}$, with $\vec{G}$ a reciprocal lattice vector such that $\langle \rho_{\rm s}(\vec{Q}_{\rm s}) \rangle = \langle \rho_{\rm s}(-\vec{Q}_{\rm s}) \rangle = \overline{\langle \rho_{\rm s}(\vec{Q}_{\rm s}) \rangle}$. Hence, the order parameter is real and the phase is pinned to zero. In the other extreme of incommensurability ($M\vec{Q} \neq \vec{G}$ for all integer values of M), it is known that the phase is not pinned [9]. At $\delta = 0.2$ we have $M\vec{Q}_{\rm s} = \vec{G}$ with $M = 10$. To estimate the magnitude

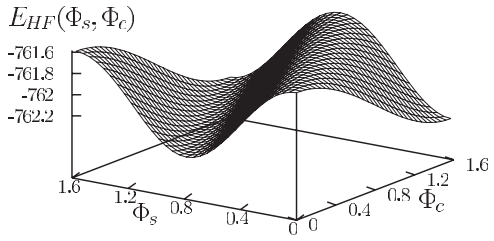

Fig. 5 – Hartree-Fock energy for a spin and charge density wave ansatz on a 30×8 lattice at $U/t = 3$ and $\delta = 0.2$ (see text). For each value of the phases, we solve the mean-field self-consistent equations for the moduli of the order parameters.

of the pinning we solve the mean-field self-consistent equations for the moduli of the order parameters at fixed values of the phases. The thus obtained mean-field energy is plotted in fig. 5 and may be well fitted to the form $E^{\mathrm{HF}} = E_0^{\mathrm{HF}} + A_1 \cos^2(\Phi_1 + \pi/2) + A_2 \cos^2(\Phi_2)$, where $\Phi_1 = 2\Phi_{\mathrm{c}} + \Phi_{\mathrm{s}}$ and $\Phi_2 = -\Phi_{\mathrm{c}} + 2\Phi_{\mathrm{s}}$. For the $L_y = 8$ and $L_x = 30$ system at $\delta = 0.2$ we find that $A_1 \simeq -5 \times 10^{-5}$, while $A_2 \simeq 0.8t$. This implies that the pinning of the Φ_1 mode is extremely small since it is proportional to $\sqrt{A_1}$. Following this point of view for the interpretation of the data, we will have to assume that the mass of the Φ_1 mode is beyond our numerical resolution so that we are not able to distinguish it from a genuine Goldstone mode. Pinning $\Phi_2 = \pi/2$ and recalling that $\Phi_1 = 2\Phi_{\mathrm{c}} + \Phi_{\mathrm{s}}$, and $2\vec{Q}_{\mathrm{c}} = \vec{Q}_{\mathrm{s}}$ locks together the dynamics of the spin and charge density wave. The QMC results of fig. 4 support this point of view, since the velocities of the spin and charge modes are comparable. Within this interpretation the conductivity data reflects the siding mode of the charge-density wave.

We have up to now concentrated on *narrow* rectangular lattices where the topology forces stripes to occur along only one direction. As the width of the system increases to approach a square topology, peaks in the structure factors are seen along both lattice directions. Figure 6 plots the spin and charge structure factors for our largest system: $L_y = 10$, $L_x = 30$. The spin shows pronounced features not only at $(\pi - \epsilon_x, \pi)$ but also at $(\pi, \pi - \epsilon_y)$, where $\epsilon_x = \pi\delta$ and $\epsilon_y = 2\pi/L_y$. In the charge sector, cusps are seen at $(2\epsilon_x, 0)$ and $(0, 2\epsilon_y)$. At each of those wave vectors, and as partially shown in fig. 4, soft modes in the dynamical spin and charge structure factors are apparent. On this lattice topology, it is possible to arrange the holes in

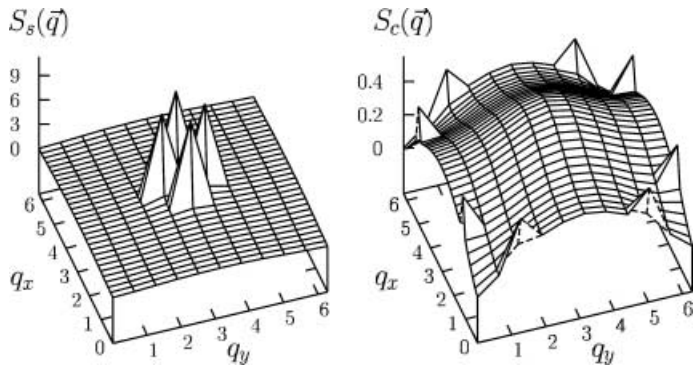

Fig. 6 – Ground-state spin ($S_{\mathrm{s}}(\vec{q})$) and charge ($S_{\mathrm{s}}(\vec{q})$) static structure factors at $U/t = 3$, $\delta = 0.2$ and on a 30×10 lattice.

two stripes along the x-direction or in five stripes along the y-direction. If the stripe ordering turns out to be long-ranged, one expects one of the two directions to be spontaneously chosen in the thermodynamic limit. On the other hand, if there is no long-range stripe order, just short-range fluctuations, we expect this state to remain stable as the size of the system grows.

To summarize, we have introduced a new QMC approach which allows us to obtain insight into doped Mott insulators. It is based on the observation that when the number of fermion flavors $N = 4n$, a broken spin-symmetry Hubbard model may be simulated with no sign problem, regardless of the lattice topology and band filling. More generally, as a function of growing values of N, the sign problem becomes less and less severe. Our approach clearly provides a way to go beyond Gaussian fluctuations around a given saddle point. On the other hand, it is at present not clear if the extrapolation from finite N to $N = 2$ is justified. We have used this method to investigate the doped Mott insulator at $N = 4$. We find a metallic state with no quasiparticles, since there is a gap or pseudo-gap in the single-particle density of states. The low-energy excitations are collective spin and charge modes. On our largest rectangular topologies they are *gapless* in the spin sector at $(\pi \pm \epsilon_x, \pi)$ and $(\pi, \pi \pm \epsilon_y)$ and at $(\pm 2\epsilon_x, 0)$, $(0, \pm 2\epsilon_y)$, $(0, 0)$ in the charge sector. ϵ_x and ϵ_y depend on doping and lattice topology.

* * *

We wish to thank the HLR-Stuttgart for generous allocation of computer time, the DFG for financial support (grant numbers AS 120/1-3, AS 120/1-1) as well as a joint Franco-German cooperative grant (PROCOPE). FFA thanks P. Horsch and R. Zeyher for discussions. We thank R. Scalettar for a critical reading of the manuscript.

REFERENCES

[1] Emery V., Kivelson S. and Tranquada J., *Proc. Natl. Acad. Sci. USA*, **96** (1999) 8814.
[2] Klauss H. H., Wagener W., Hillberg M., Kopmann W., Walf H., Litterst F. J., Hücker M. and Büchner B., *Phys. Rev. Lett.*, **85** (2000) 4590.
[3] Capponi S. and Assaad F. F., *Phys. Rev. B*, **63** (2001) 155113.
[4] Jarrell M. and Gubernatis J., *Phys. Rep.*, **269** (1996) 133.
[5] Parola A., Sorella S., Parrinello M. and Tosatti E., *Phys. Rev. B*, **43** (1991) 6190.
[6] Auerbach A., *Interacting Electrons and Quantum Magnetism, Graduate Texts in Contemporary Physics* (Springer, New York, Berlin, Heidelberg) 1994.
[7] Eskes H., Meinders M. B. J. and Sawatzky G. A., *Phys. Rev. Lett.*, **67** (1991) 1035.
[8] Voit J., *Rep. Prog. Phys.*, **57** (1994) 977.
[9] Lee P., Rice T. and Anderson P., *Solid State Commun.*, **14** (1974) 703.
[10] Grüner G., *Rev. Mod. Phys.*, **66** (1994) 1.